Atmos. Chem. Phys. Discuss., 15, 11495–11524, 2015
www.atmos-chem-phys-discuss.net/15/11495/2015/
doi:10.5194/acpd-15-11495-2015

Atmospheric Chemistry and Physics
Discussions
Open Access

Particle hygroscopicity and its link to chemical composition in the urban atmosphere of Beijing, China during summertime

Z. J. Wu[1], **J. Zheng**[1], **D. J. Shang**[1], **Z. F. Du**[1], **Y. S. Wu**[1], **L. M. Zeng**[1], **A. Wiedensohler**[2], **and M. Hu**[1]

[1]State Key Joint Laboratory of Environmental Simulation and Pollution Control, College of Environmental Sciences and Engineering, Peking University, Beijing 100871, China
[2]Leibniz Institute for Tropospheric Research, 04318 Leipzig, Germany

Received: 8 March 2015 – Accepted: 26 March 2015 – Published: 20 April 2015

Correspondence to: M. Hu (minhu@pku.edu.cn) and Z. J. Wu (zhijunwu@pku.edu.cn)

Published by Copernicus Publications on behalf of the European Geosciences Union.

Abstract

Simultaneous measurements of particle number size distribution, particle hygroscopic properties, and size-resolved chemical composition were made during the summer of 2014 in Beijing, China. During the measurement period, the median hygroscopicity parameters (κ) of 50, 100, 150, 200, and 250 nm particles are respectively 0.15, 0.19, 0.22, 0.27, and 0.29, showing an increasing trend with increasing particle size. When $PM_{2.5}$ mass concentration is greater than $50\,\mu g\,m^{-3}$, the fractions of the hydrophilic mode for 150, 250, 350 nm particles increased towards 1 as $PM_{2.5}$ mass concentration increased. This indicates that aged particles dominated during severe pollution periods in the atmosphere of Beijing. Particle hygroscopic growth can be well predicted using high time-resolution size-resolved chemical composition derived from AMS measurement on a basis of ZSR mixing rule. An empirical relationship between κ of organic fraction (κ_{org}) and oxygen to carbon ratio (O : C) ($\kappa_{org} = 0.08 \cdot O : C + 0.02$) is obtained. During new particle formation event associating with strongly active photochemistry, the hygroscopic growth factor or κ of newly formed particles is greater than for particle with the same sizes during non-NPF periods. A quick transformation from external mixture to internal mixture for pre-existing particles (for example 250 nm particle) was observed. Such transformations can modify the state of mixture of pre-exiting particles and thus modify properties such as the light absorption coefficient and cloud condensation nuclei activation.

1 Introduction

Hygroscopic growth of atmospheric particles is one of the important parameters controlling their direct and indirect climate effects (McFiggans et al., 2006; Haywood and Boucher, 2000). Due to water uptake, hydrophilic particles grow significantly in size at high relative humidity (RH), which influences the particle light scattering and extinction coefficients, thereby impairing visibility (Sloane and Wolff, 1985). In addition, the water content of atmospheric aerosol particles can serve as a site for heterogeneous nucleation and reactions that perturb local photochemistry (Kreidenweis and Asa-Awuku, 2014). Therefore, a better understanding of hygroscopic behavior of atmospheric aerosol particle is required to further elucidate the physicochemical processes in the atmosphere.

The association of the particle chemical composition with their size-dependent hygroscopic behavior is rather complex. In order to overcome such complexities, Petters and Kreidenweis (2007) proposed a single hygroscopic parameter (κ), namely κ-Köhler theory. On the basis of the κ-Köhler theory and Zdanovskii–Stokes–Robinson (ZSR) mixing rule (Stokes and Robinson, 1966; Zdanovskii, 1948), particle hygroscopic growth of a homogeneous chemical mixture can be predicted, knowing hygroscopic growth factors of pure chemical species. Aerosol mass spectrometers (AMS), which have been increasingly deployed in atmospheric aerosol studies, can provide a high time resolution of the size-resolved chemical composition of non-refractory particle material (DeCarlo et al., 2006). Therefore, coupled measurements of an AMS and a Hygroscopicity Tandem Differential Mobility Analyzer (HTDMA) are able to capture highly variable changes in chemical particle composition and hygroscopicity in real time. Recently, some studies highlighted the advantage of using size-selected AMS information over size-averaged information from off-line chemical characterization (Medina et al., 2007; Gunthe et al., 2009; Cerully et al., 2011; Wu et al., 2013).

Another key product of AMS measurements is the oxidation level and chemical information of organic aerosol particles. Compared to inorganic species, which exhibit a well-characterized hygroscopic behavior, knowledge on the influence of the water uptake of the organic aerosol particle fraction remains limited (Kanakidou et al., 2005; Hallquist et al., 2009). The hygroscopicity of organic aerosol material varies with its oxidation state (Jimenez et al., 2009), which may be highly variable in the real atmosphere, depending on the history of an air mass. Such variation may present a significant challenge when predicting hygroscopicity assuming a constant hygroscopic growth factor of the organic aerosol fraction at a given relative humidity, as has usually been done in closure studies.

Over the past several decades, particle hygroscopicity measurements have been carried out world-wide, using the HTDMA technique. Atmospheric environments, in which those measurements were performed includes marine, Antarctic, boreal forest, rural, and urban areas. Swietlicki et al. (2008) and Kreidenweis and Asa-Awu (2014) compiled the existing observations on particle hygroscopic growth in the literature. Throughout these compilations, measurements of particle hygroscopicity have been rarely performed in China, which experiences frequently severe haze pollution episodes. These few particle hygroscopicity measurements using the HTDMA technique were deployed in Yangtze River Delta (Shanghai, Ye et al., 2013, and Hangzhou, Zhang et al., 2011), Pearl River Delta (Xinken, Cheng et al., 2008 and Hong Kong, Lopez-Yglesias et al., 2014) and North China Plain (Beijing, Massling et al., 2009, and Wuqing, Liu et al., 2011). Unfortunately, these measurements lack a linkage between particle hygroscopicity and chemical composition.

This study investigates the size-resolved particle hygroscopicity and chemical composition in Beijing, China, during summertime. Our work provides a general overview of particle hygroscopic behavior as well as a comparison of the observed and simulated hygroscopic particle growth using AMS-based chemical particle composition, emphasizing on the organic mass fraction. Additionally, the evolution of particle hygroscopicity during new particle formation event is investigated to understand the effects of strong photochemistry-driven atmospheric oxidation processes on particle hygroscopicity and mixing state.

2 Experimental procedure

2.1 Sampling site

The sampling site is on the campus of Peking University, located in northwest Beijing. The laboratory is equipped with a suit of aerosol instruments sites on the roof of a building (20 m above the ground). The relative humidity (RH) of the sampled air was kept to below 30 % using silica gel dryer and Nafion dryer in series. The particle number size distribution, particle hygroscopicity, and aerosol mass spectroscopic measurements were concurrently made. Particle number size distribution is measured by TSI-SMPS (Long-DMA3081+CPC3775 and Nano-DMA3085+UCPC3776). The multiple charge correction and particle loss correction are carried out. Other core instruments will be briefly described below. Additionally, a weather station (Met One Instruments Inc.) provides the meteorological parameters.

2.2 Instrumentation

The HTDMA used in this study has been described in detail in previous publications (Wu et al., 2011; Massling et al., 2003), and complies to the instrumental standards and quality assurance prescribed in Massling et al. (2011). The HTDMA consists of three main parts: (1) a Differential Mobility Analyzer (DMA1) that selects quasi-monodisperse particles, and a Condensation Particle Counter (CPC1) that measures the particle number concentration leaving the DMA1 at the selected particle size, (2) an aerosol humidifier conditioning the particles selected by DMA1 to a defined relative humidity (RH), (3) the second DMA (DMA2) coupled with another condensation particle counter (CPC2) to measure the number size distributions of the humidified aerosol. The second DMA and the aerosol humidification are placed in a temperature-controlled box. Hygroscopicity scans with 100 nm ammonium sulfate particles were performed every 3 h to analyze the stability of the relative humidity of 90 % in the second DMA. Hygroscopicity scan with a deviation of more than 3 % in relative humidity to the set-point of 90 % will not be considered for further analysis.

The hygroscopic growth factor (HGF) is defined as the ratio of the particle mobility diameter, $D(\mathrm{RH})$, at a given RH to the dry diameter, $D_{\mathrm{p_{dry}}}$:

$$\mathrm{HGF(RH)} = \frac{D_{\mathrm{p}}(\mathrm{RH})}{D_{\mathrm{p_{dry}}}} \tag{1}$$

The TDMA*inv* method developed by Gysel et al. (2009) was used to invert the HTDMA data. Dry scans (under $\mathrm{RH} < 10\,\%$) are used to calibrate a possible offset between DMA1 and DMA2 and define the width of the HTDMA's transfer function (Gysel et al., 2009).

Based on the ZSR method, the HGF of a mixture can be estimated from the HGF_i of the pure components and their respective volume fractions, ε_i (Malm and Kreidenweis, 1997):

$$\mathrm{HGF_{mixed}} = \left(\sum_i \varepsilon_i \mathrm{HGF}_i^3\right)^{1/3} \tag{2}$$

Here, we assume that two components including soluble and insoluble fractions consist of aerosols (also refer to Ehn et al., 2007; Swietlicki et al., 1999). The soluble fraction is assumed to be ammonium sulfate. Then, ε of soluble fraction can be calculated by:

$$\varepsilon_{\mathrm{soluble}} = \frac{\mathrm{HGF}^3_{\mathrm{measured}} - 1}{\mathrm{HGF}^3_{\mathrm{(HN_4)_2SO_4}} - 1} \tag{3}$$

where $\mathrm{HGF_{measured}}$ is the HGF of the particles measured by HTDMA, and $\mathrm{HGF_{(HN_4)_2SO_4}}$ is the HGF of pure $(\mathrm{NH_4})_2\mathrm{SO_4}$ particles with the same size. When calculating $\mathrm{HGF_{(HN_4)_2SO_4}}$ in different diameters, the parameterizations for $(\mathrm{NH_4})_2\mathrm{SO_4}$ water activity developed by Potukuchi and Wexler (1995) and the density reported by Tang and Munkelwitz (1994) are used. The Kelvin term was considered in the calculation.

2.3 Particle chemical composition

The Aerodyne HR-ToF-AMS (here simply referred to as AMS) (DeCarlo et al., 2006) was operated with a time resolution of 5 min. 0.5 is taken as the AMS collection efficiency. Due to the 600 °C surface temperature of the vaporizer, the AMS can only analyze the non-refractory chemical composition of the particles. Elemental carbon, crustal material, and sea-salt cannot be detected. Therefore, based on the transmission efficiency of the aerodynamic lenses and the detected compounds, the AMS can provide the size-resolved chemical composition of the submicrometer non-refractory aerosol particle fraction (NR-PM_1) (Canagaratna et al., 2007). Applying the method developed by Canagarantna et al. (2015) the high resolution organic particle mass spectra were used to determine the elemental composition and the Oxygen to Carbon atomic ratio (O : C). The vacuum aerodynamic diameter for AMS measurements was converted to the volume equivalent particle diameter by division of AMS vacuum aerodynamic diameter by the estimated particle density (1500 kg m^{-3}). Hereafter, the mobility diameter (assuming spherical particles) was used for AMS data below.

AMS-positive matrix factor (PMF) analysis was performed to identify different organic aerosols (OA) factors based on the high resolution mass spectra of organics (Ulbrich et al., 2009). Four OA components were resolved by PMF, including low-volatility oxygenated organic aerosol (LV-OOA), semi-volatile oxygenated OA (SV-OOA), hydrocarbon-like OA (HOA) and cooking OA (COA). LV-OOA and SV-OOA typically represented aged SOA and freshly formed SOA, respectively (Ulbrich et al., 2009). HOA and COA were both anthropogenic primary organic aerosol (POA) components (Huang et al., 2010).

Black carbon (BC) mass concentration in µg m^{-3} is derived from Photoacoustic Extinctiometer (PAX) measurements (Patrick Arnott et al., 1999) equipped with PM_1 cut-off inlet. In this study, PAX measurements were performed at wavelength 532 nm.

3 Theory

3.1 Hygroscopicity parameter

The hygroscopicity parameter, κ, can be calculated from the hygroscopic growth factor (HGF) measured by HTDMA (Petters and Kreidenweis, 2007):

$$\kappa_{\mathrm{HTDMA}} = (\mathrm{HGF}^3 - 1)\left(\frac{\exp\left(\frac{A}{D_{\mathrm{p_{dry}}}\cdot\mathrm{HGF}}\right)}{\mathrm{RH}} - 1\right) \tag{4}$$

$$A = \frac{4\sigma_{\mathrm{s/a}}M_{\mathrm{w}}}{RT\rho_{\mathrm{w}}} \tag{5}$$

Where $D_{\mathrm{p_{dry}}}$ and HGF are the initial dry particle diameter and the hygroscopic growth factor at 90 % RH measured by HTDMA, respectively. $\sigma_{\mathrm{s/a}}$ is the droplet surface tension (assumed to be that of pure water, $\sigma_{\mathrm{s/a}} = 0.0728\,\mathrm{N\,m^{-2}}$), M_{w} the molecular weight of water, ρ_{w} the density of liquid water, R the universal gas constant, and T the absolute temperature.

For a given internal mixture, κ can also be predicted by a simple mixing rule on the basis of chemical volume fractions ε_i (Petters and Kreidenweis, 2007):

$$\kappa_{\mathrm{chem}} = \sum_i \varepsilon_i \kappa_i \tag{6}$$

Here, κ_i and ε_i are the hygroscopicity parameters and volume fraction for the individual (dry) component in the mixture with i the number of components in the mixture. We derive ε_i from the particle chemical composition measured by AMS and PAX. The detailed description of how to calculate volume fraction is given in Sect. 3.2. In the following discussions, κ_{HTDMA} and κ_{chem} denote respectively the values derived from HTDMA and predicted using ZSR mixing rule.

3.2 Hygroscopicity-chemical composition closure

The AMS provides the particle mass size distribution of sulfate (SO_4^{2-}), nitrate (NO_3), and ammonium (NH_4^+) ions as well that of organic compounds. We use a simplified ion pairing scheme as presented in Gysel et al. (2007) to convert the ion mass concentrations to the mass concentrations of their corresponding inorganic salts as listed in Table 1. Unlike inorganic salts, the hygroscopicity of organic aerosols is not well-recognized. In the literature, there are different approaches in representing κ_{org} in the closure studies. Typically, κ_{org} is assumed as a constant value. Chang et al. (2010) represented κ_{org} by using the factors from the PMF analysis to group organics measured by AMS into two components: a non-hygroscopic, unoxygenated component consisting of the hydrocarbon-like organic aerosol (HOA) factor and a hygroscopic component, consisting of the oxygenated factors LV-OOA, SV-OOA, and biomass burning organic aerosol (BBOA). In our study, organic materials derived from AMS measurements are grouped into two components including secondary organic aerosols (SOA) and primary organic aerosols (POA) based on AMS-PMF analysis. SOA, including LV-OOA and SV-OOA factors, is a more oxygenated organic aerosol, thereby more hygroscopic and has a κ_{SOA} of 0.1, which was calculated from the hygroscopic growth factor of organics at 90 % RH as given in Gysel et al. (2007) using Eq. (4). POA is the unoxygenated component consisting of the HOA and COA factors and is treated as hydrophobic material with $\kappa_{\text{POA}} = 0$. Then, κ_{org} can be calculated as:

$$k_{\text{org}} = f_{\text{POA}} \cdot k_{\text{POA}} + f_{\text{SOA}} \cdot k_{\text{SOA}} \quad (7)$$

Here, κ_{org} is overall κ for organic aerosols. f_{POA} and f_{SOA} are volume fraction of POA and SOA in total organic aerosols measured by AMS.

The volume fraction of each species was calculated from the particle mass concentration divided by its density as given in Table 1. The densities for inorganic salts are well defined. By summarizing the articles published (Park et al., 2004; McMurry et al., 2002; Kondo et al., 2011; Kiselev et al., 2010), 1700 $\text{kg}\,\text{m}^{-3}$ was selected as BC density. The hygroscopicity parameter κ of the hydrophobic black carbon was considered to be zero. The density of organic particle mass fraction including both SOA and POA was taken to be 1400 kg m^{-3} (Gysel et al., 2007; Alfarra et al., 2006; Dinar et al., 2006).

4 Results and discussion

4.1 Overview of particle hygroscopic growth and the mixing state

The sampling period spans from 31 May to 24 June 2014. Figure 1 provides an overview of the particle number size distribution, meteorological parameters, the chemical composition of NR-PM$_1$, and hygroscopicity parameters (κ) during the entire field campaign. The ambient temperature typically is above 30 °C during daytime and around 2 °C during nighttime, as displayed in Fig. 1b. The mean RH is 53 ± 17 %, and frequently above 70 % during nighttime. Compared to other seasons in Beijing, the photochemical and biological activities are enhanced during high temperature and high humidity periods in summer. As shown in the Fig. 1a, new particle formation (NPF) events are observed frequently during the sampling period, accounting for 54 % of the measuring days.

The hygroscopicity of aerosol particles with diameters of 50, 100, 150, 250, and 350 nm were measured at RH = 90 %. As examples, Fig. 1c displays the time series of hygroscopicity parameters for 50 nm ($\kappa_{50\,\mathrm{nm}}$) and 250 nm ($\kappa_{250\,\mathrm{nm}}$) particles. Both $\kappa_{50\,\mathrm{nm}}$ and $\kappa_{250\,\mathrm{nm}}$ have an obvious temporal variability, which is similar to that of inorganic mass fraction in NR-PM$_1$ displayed in Fig. 1d. Figure 2 (left) shows the size-dependent particle hygroscopicity parameters and inorganic mass fraction of NR-PM$_1$ derived from averaging over the entire measuring period. The particle hygroscopicity increases with increasing particle size, displaying the same size-dependency with the mass fraction of inorganic composition in NR-PM$_1$. This is because inorganics including ammonium sulfate and ammonium nitrate are major water-soluble chemical compounds in the atmospheric particles. Compared to inorganic components, the hygroscopicity parameter of organic aerosols are typically lower than 0.1 (Varutbangkul et al., 2006; Virkkula et al., 1999).

During the sampling period, the growth factor probability density function (GF-PDF) shows two distinct modes, which are identified as hydrophobic mode ($GF < 1.2$) and hydrophilic mode ($GF > 1.2$). Figure 2 (right) shows the size-dependency of the fraction of the hydrophilic mode. It can be seen that the hydrophilic mode is more prominent, no matter what particle size is considered. With increasing particle size, the dominance of hydrophilic mode becomes more pronounced. Above 150 nm, the number fraction of hydrophilic mode is around 0.8, and its size-dependency is insignificant. Below 150 nm, the number fraction of hydrophilic mode increases significantly with increasing particle size. The median number fraction of hydrophilic mode for 50 nm particles is 0.6, which is smaller than those of larger particles. Larger particles (here, above 150 nm) constituting a larger fraction of the hydrophilic mode can be explained as such: in the urban area, traffic emissions are major sources for particles below 100 nm. Typically, freshly emitted particles, such as soot, are initially hydrophobic and externally mixed. In contrast, larger particles have undergone atmospheric aging processes during transport (such as coagulation, condensation, chemical reaction) (Pöschl, 2005) for a longer time. These aging processes enhance the particle's water solubility (Pöschl, 2005; Jimenez et al., 2009) and result in more internally mixed particles.

The haze issue caused by high aerosol loadings over the northern plain of China is a major concern, for both air quality and climate effects. Here, the $PM_{2.5}$ mass concentration, a key factor characterizing air pollution, vs. the fraction of the hydrophilic mode is plotted (Fig. 3) to analyze the relationship between particle mixing state and air pollution. There is no obvious dependency between the $PM_{2.5}$ mass concentration and the number fraction of hydrophilic mode for 50 nm particles, which can be expected due to the low mass fraction of ultrafine particles. This is however also true for 150, 250, and 350 nm particles, if $PM_{2.5}$ mass concentration is lower than 50 $\mu g\, m^{-3}$. The reason for this is that the particle mass concentration is dominated by local sources and less by secondary aerosol particles formed during long-range transport. Conversely, when

$PM_{2.5}$ mass concentration is larger than 50 µg m^{-3}, the fraction of the hydrophilic mode is larger than 0.7. With the increasing $PM_{2.5}$ mass concentration, the fraction rises towards to 1, indicating that the aged aerosols are dominant. This means that secondary aerosol particles are dominant during severe particulate pollution episodes, occurring frequently in Beijing. Our results are consistent to recent scientific findings (Guo et al., 2014; Huang et al., 2014), which pointed out that the haze pollution events were mainly attributable to secondary aerosol formation.

4.2 Closure between particle hygroscopicity and chemical components

The AMS-derived particle mass concentrations for different chemical compounds are used to perform a closure study. The particle mass concentrations for individual species are integrated over the size interval of $D_{p_{dry}} \pm 50$ nm. Here, $D_{p_{dry}}$ is the dry particle diameter selected by HTDMA. Considering the limited signal statistics in this narrow size range, AMS data are used to carry out the closure only if the sum of sulfate, nitrate, ammonium, and organics mass concentrations derived from integrating size range of $D_{p_{dry}} \pm 5$ nm is greater than 1 µg m^{-3}.

The BC particle mass concentration within the size range of $D_{p_{dry}} \pm 50$ nm was estimated as follows: first, the ratio (R_{BC/PM_1}) of BC particle mass concentration (derived from PAX) to bulk particle mass concentration (derived from AMS measurement) is calculated, assuming this ratio is independent on the particle size. Afterwards, the BC particle mass concentration in a certain size range, e.g., 150 ± 50 nm is estimated by multiplying the mass concentration derived from integrating particle size range of 150 ± 50 nm (AMS data) and R_{BC/PM_1}. One should note that this assumption may give an uncertainty in the closure, because the BC mass concentration has a dependency with particle size (Huang et al., 2006).

The SOA and POA mass fractions within the size range of $D_{p_{dry}} \pm 50$ nm are estimated using a similar method as the calculation of BC mass concentration given above. The POA (MF_{POA}) and SOA (MF_{SOA}) mass fractions in total organic aerosols in NR-PM_1 are calculated on a basis of the AMS-PMF analysis results. Assuming MF_{POA} and MF_{SOA} are independent of the particle diameter, the POA or SOA mass concentration in the size range $D_{p_{dry}}$ ±5 nm can be calculated by multiplying the organic mass concentration derived from integrating particle size range of 150 ± 50 nm (AMS data) and MF_{POA} or MF_{SOA}.

Figure 4 shows the scattering plots of κ_{chem} calculated based on the size-resolved chemical composition against κ_{HTDMA}. The fitted slopes for 150, 25, and 350 nm particles are 1.02, 0.99, and 0.97, respectively, which is close to unit. This indicates that the measured κ can be well predicted on a basis of AMS data and the ZSR mixing rule.

Assuming the inorganic fraction is fully explained by the ZSR mixing rule, κ_{org} can be calculated by subtracting κ of inorganic fraction and BC from κ_{HTDMA}. Here, κ_{org} for 150 nm particles is calculated because it provides a better closure result and higher organic fraction in contrast to other particle sizes. Duplissy et al. (2011) pointed out that the uncertainty in the estimation of κ_{org} decreases with increasing organic fraction, thereby, only data featuring organic fractions larger than 50 % are used in this calculation. In addition, the evaporation of NH_4NO_3 could occur in the DMAs and the humidification section. This leads to a positive prediction bias because the volatile NH_4NO_3, which is fully detected by AMS, can evaporate in the HTDMA system (Gysel et al., 2007). Here, only data with NH_4NO_3 volume fraction below 20 % are considered in order to reduce the evaporation artifact of NH_4NO_3. Figure 5 shows κ_{org} as a function of O : C ratio. A clear correlation between κ_{org} and the O : C ratios is not obtained. Several previous studies reported the similar plots of κ_{org} values as a function of O : C ratios (Chang et al., 2010; Bhattu and Tripathi, 2015). In order to derive an empirical relationship between κ_{org} and O : C ratios, κ_{org} values are binned by O : C in increments of 0.1. As displayed in Fig. 5, a linear fitting function ($\kappa_{org} = 0.08 \cdot \mathrm{O:C} + 0.02$) is obtained. Some empirical functions reported by other previous studies are also shown in Fig. 5. We note that the slopes of linear fitting varied with different studies. In this study and Wu et al. (2013), κs of organics derived from HTDMA are used to correlate with the O : C ratio. Differently, κs from CCN counter measurements in Chang et al. (2010) and

Title Page
Abstract | Introduction
Conclusions | References
Tables | Figures
◀| |▶
◀ ▶
Back | Close
Full Screen / Esc
Printer-friendly Version
Interactive Discussion

Mei et al. (2013) are taken. Due to the discrepancy between the κs derived from HTDMA and CCN counter (Irwin et al., 2010), the same dataset may produce a different relationship between O : C ratio and κ_{org}. We should also note that the different aerosol formation ways in different environments could also be an explanation for the different relationship between κ_{org} and O : C.

4.3 Case study: particle hygroscopic behavior during NPF events

As shown in Fig. 1, NPF events frequently took place during the sampling period. In order to understand the effects of NPF on particle hygroscopic behavior, this section will exemplify the evolution of particle hygroscopicity during a NPF event. Figure 6 displays the time series of particle number size distribution and GF-PDF during a NPF event occurred on 5 June 2014. A typical new particle formation event starts at 11 a.m. (local time) on 5 June, and continues to grow until 6 a.m. on 6 June 2014. Meanwhile, the newly formed particles grew to a particle size of approximately 100 nm. In Fig. 6, the GF-PDF and water soluble fraction of 50 and 250 nm particles are shown. The former (50 nm particles) represents the newly formed particles, and the latter (250 nm particles) represents the pre-existing particles.

As displayed in Fig. 6a, the particle formation starts at 9.50 p.m. (local time) and the newly formed particles reach to particle size of 50 nm at 12.30 p.m. Meanwhile, an obvious enhancement in hygroscopicity of 50 nm particles takes place. The fraction of the hydrophilic mode particles increased from 0.5 to 1, showing the conversion of externally to more internally mixed particles. The water soluble fraction of 50 nm new particle is 42 %. This indicates that 42 % of the chemical species contributing new particle growth to 50 nm are water soluble. The water soluble chemical component may mainly be ammonium sulfate formed from neutralization reaction between ammonia and sufuric acid, which is a well-recognized chemical species contributing to particle formation and growth. The rest is secondary organic compounds, which are typically have low water solubility. Around 8.30 p.m., the fraction of the hydrophilic mode particles dropped to 0.6, and hydrophilic mode appeared again. This is attributed to the intensive traffic emissions at the time of rush hour, which can clearly be seen from the particle number size distribution. We also note that the growth factor of hydrophilic mode particles decrease during the night. This can be explained by sulfuric acid condensation playing a minor role in particle growth during the night. Simultaneously, ambient temperature decreased from 27 to 20 °C. Lower temperature facilitates the condensation of semi-volatile organic vapors onto the newly formed particles.

The 250 nm particles, which are considered pre-existing particles, have a large surface area compared to smaller (for example, particles smaller than 100 nm) and larger particles (for example, particles larger than 350 nm). As shown in Fig. 6c, the fraction of the hydrophilic mode particles increased significantly and approached 1 after the starting of NPF event. This can be explained as such: during the particle formation, a large amount of condensable vapors, such as sulfuric acid and secondary organic species are produced because of the strongly active photochemistry. These condensable vapors can condense onto the pre-existing particle and result in the transformation of external mixture to internal mixture. Such transformation may alter the atmospheric behaviors of pre-exiting particles, such as optical property and cloud condensation nuclei activation during the new particle formation events.

5 Conclusions

Particle number size distribution, particle hygroscopicity, and size-resolved chemical composition were measured concurrently during summertime 2014 in Beijing, China. The particle hygroscopicity showed a pronounced size-dependency. It increases with increasing particle size. During the measurement period, the median κs of 50, 100, 150, 200, and 250 nm particles are 0.15, 0.19, 0.22, 0.27, and 0.29, respectively. The hydrophilic mode (HGF > 1.2) is more prominent, no matter what particle size is considered. With increasing particle size, the dominance of hydrophilic mode becomes more pronounced. When $PM_{2.5}$ mass concentration is below 50 $\mu g\,m^{-3}$, no dependency between $PM_{2.5}$ mass concentration and the number fraction of hydrophilic mode is found.

Above 50 µg m^{-3}, the number fraction of hydrophilic mode for 150, 250, 350 nm particles increases and rises towards to 1 with the increasing $PM_{2.5}$ mass concentration. This means that aged particles dominate the particle mass concentration, especially during severe particulate pollution events in Beijing. Based on the size-resolved AMS data, the particle hygroscopic growth can be well predicted using the ZSR method. An empirical relationship between κ_{org} and O : C ratio ($\kappa_{org} = 0.08 \cdot \mathrm{O:C} + 0.02$) is obtained.

Frequent new particle formation events took place during the measuring period (Frequency is 54 %). The hygroscopic growth factor or κ of newly formed particles is greater than the hygroscopic growth factor of particles with the same sizes during non-NPF periods. During the new particle formation, fast transformations of external mixture to internal mixture for existing particles (for example 250 nm particle) have been observed. This is a strong indication that secondary aerosol material such as organics and sulfates were produced due to the strongly active photochemistry during NPF events, and subsequently condensed onto the particles. Such transformation may modify the atmospheric behaviors of pre-exiting particles, such as optical property and cloud condensation nuclei activation.

Acknowledgements. This work is supported by the following projects: National Natural Science Foundation of China (41475127), National Basic Research Program of China (2013CB228503), Special Fund of State Key Joint Laboratory of Environment Simulation and Pollution Control (14L02ESPC), and the China Ministry of Environmental Protection's Special Funds for Scientific Research on Public Welfare (201409010). The authors would like to thank Douglas R. Worsnop for useful discussion about the AMS size distribution data processing.

References

Alfarra, M. R., Paulsen, D., Gysel, M., Garforth, A. A., Dommen, J., Prévôt, A. S. H., Worsnop, D. R., Baltensperger, U., and Coe, H.: A mass spectrometric study of secondary organic aerosols formed from the photooxidation of anthropogenic and biogenic precursors in a reaction chamber, Atmos. Chem. Phys., 6, 5279–5293, doi:10.5194/acp-6-5279-2006, 2006.

Bhattu, D. and Tripathi, S. N.: CCN closure study: effects of aerosol chemical composition and mixing state, J. Geophys. Res.-Atmos., 120, 766–783, doi:10.1002/2014JD021978, 2015.

Canagaratna, M. R., Jayne, J. T., Jimenez, J. L., Allan, J. D., Alfarra, M. R., Zhang, Q., Onasch, T. B., Drewnick, F., Coe, H., Middlebrook, A., Delia, A., Williams, L. R., Trimborn, A. M., Northway, M. J., DeCarlo, P. F., Kolb, C. E., Davidovits, P., and Worsnop, D. R.: Chemical and microphysical characterization of ambient aerosols with the aerodyne aerosol mass spectrometer, Mass Spectrom. Rev., 26, 185–222, doi:10.1002/mas.20115, 2007.

Canagaratna, M. R., Jimenez, J. L., Kroll, J. H., Chen, Q., Kessler, S. H., Massoli, P., Hildebrandt Ruiz, L., Fortner, E., Williams, L. R., Wilson, K. R., Surratt, J. D., Donahue, N. M., Jayne, J. T., and Worsnop, D. R.: Elemental ratio measurements of organic compounds using aerosol mass spectrometry: characterization, improved calibration, and implications, Atmos. Chem. Phys., 15, 253–272, doi:10.5194/acp-15-253-2015, 2015.

Cerully, K. M., Raatikainen, T., Lance, S., Tkacik, D., Tiitta, P., Petäjä, T., Ehn, M., Kulmala, M., Worsnop, D. R., Laaksonen, A., Smith, J. N., and Nenes, A.: Aerosol hygroscopicity and CCN activation kinetics in a boreal forest environment during the 2007 EUCAARI campaign, Atmos. Chem. Phys., 11, 12369–12386, doi:10.5194/acp-11-12369-2011, 2011.

Chang, R. Y.-W., Slowik, J. G., Shantz, N. C., Vlasenko, A., Liggio, J., Sjostedt, S. J., Leaitch, W. R., and Abbatt, J. P. D.: The hygroscopicity parameter (κ) of ambient organic aerosol at a field site subject to biogenic and anthropogenic influences: relationship to degree of aerosol oxidation, Atmos. Chem. Phys., 10, 5047–5064, doi:10.5194/acp-10-5047-2010, 2010.

Cheng, Y. F., Wiedensohler, A., Eichler, H., Heintzenberg, J., Tesche, M., Ansmann, A., Wendisch, M., Su, H., Althausen, D., Herrmann, H., Gnauk, T., Brüggemann, E., Hu, M., and Zhang, Y. H.: Relative humidity dependence of aerosol optical properties and direct radiative forcing in the surface boundary layer at Xinken in Pearl River Delta of China: an observation based numerical study, Atmos. Environ., 42, 6373–6397, doi:10.1016/j.atmosenv.2008.04.009, 2008.

DeCarlo, P. F., Kimmel, J. R., Trimborn, A., Northway, M. J., Jayne, J. T., Aiken, A. C., Gonin, M., Fuhrer, K., Horvath, T., Docherty, K. S., Worsnop, D. R., and Jimenez, J. L.: Field-deployable, high-resolution, time-of-flight aerosol mass spectrometer, Anal. Chem., 78, 8281–8289, doi:10.1021/ac061249n, 2006.

Dinar, E., Mentel, T. F., and Rudich, Y.: The density of humic acids and humic like substances (HULIS) from fresh and aged wood burning and pollution aerosol particles, Atmos. Chem. Phys., 6, 5213–5224, doi:10.5194/acp-6-5213-2006, 2006.

Duplissy, J., DeCarlo, P. F., Dommen, J., Alfarra, M. R., Metzger, A., Barmpadimos, I., Prevot, A. S. H., Weingartner, E., Tritscher, T., Gysel, M., Aiken, A. C., Jimenez, J. L., Canagaratna, M. R., Worsnop, D. R., Collins, D. R., Tomlinson, J., and Baltensperger, U.: Relating hygroscopicity and composition of organic aerosol particulate matter, Atmos. Chem. Phys., 11, 1155–1165, doi:10.5194/acp-11-1155-2011, 2011.

Ehn, M., Petäjä, T., Aufmhoff, H., Aalto, P., Hämeri, K., Arnold, F., Laaksonen, A., and Kulmala, M.: Hygroscopic properties of ultrafine aerosol particles in the boreal forest: diurnal variation, solubility and the influence of sulfuric acid, Atmos. Chem. Phys., 7, 211–222, doi:10.5194/acp-7-211-2007, 2007.

Gunthe, S. S., King, S. M., Rose, D., Chen, Q., Roldin, P., Farmer, D. K., Jimenez, J. L., Artaxo, P., Andreae, M. O., Martin, S. T., and Pöschl, U.: Cloud condensation nuclei in pristine tropical rainforest air of Amazonia: size-resolved measurements and modeling of atmospheric aerosol composition and CCN activity, Atmos. Chem. Phys., 9, 7551–7575, doi:10.5194/acp-9-7551-2009, 2009.

Guo, S., Hu, M., Zamora, M. L., Peng, J., Shang, D., Zheng, J., Du, Z., Wu, Z., Shao, M., Zeng, L., Molina, M. J., and Zhang, R.: Elucidating severe urban haze formation in China, P. Natl. Acad. Sci. USA, 111, 17373–17378, doi:10.1073/pnas.1419604111, 2014.

Gysel, M., Crosier, J., Topping, D. O., Whitehead, J. D., Bower, K. N., Cubison, M. J., Williams, P. I., Flynn, M. J., McFiggans, G. B., and Coe, H.: Closure study between chemical composition and hygroscopic growth of aerosol particles during TORCH2, Atmos. Chem. Phys., 7, 6131–6144, doi:10.5194/acp-7-6131-2007, 2007.

Gysel, M., McFiggans, G. B., and Coe, H.: Inversion of tandem differential mobility analyser (TDMA) measurements, J. Aerosol Sci., 40, 134–151, doi:10.1016/j.jaerosci.2008.07.013, 2009.

Hallquist, M., Wenger, J. C., Baltensperger, U., Rudich, Y., Simpson, D., Claeys, M., Dommen, J., Donahue, N. M., George, C., Goldstein, A. H., Hamilton, J. F., Herrmann, H., Hoffmann, T., Iinuma, Y., Jang, M., Jenkin, M. E., Jimenez, J. L., Kiendler-Scharr, A., Maenhaut, W., McFiggans, G., Mentel, Th. F., Monod, A., Prévôt, A. S. H., Seinfeld, J. H., Surratt, J. D., Szmigielski, R., and Wildt, J.: The formation, properties and impact of secondary organic aerosol: current and emerging issues, Atmos. Chem. Phys., 9, 5155–5236, doi:10.5194/acp-9-5155-2009, 2009.

Haywood, J. and Boucher, O.: Estimates of the direct and indirect radiative forcing due to tropospheric aerosols: a review, Rev. Geophys., 38, 513–543, doi:10.1029/1999RG000078, 2000.

Huang, R.-J., Zhang, Y., Bozzetti, C., Ho, K.-F., Cao, J.-J., Han, Y., Daellenbach, K. R., Slowik, J. G., Platt, S. M., Canonaco, F., Zotter, P., Wolf, R., Pieber, S. M., Bruns, E. A., Crippa, M., Ciarelli, G., Piazzalunga, A., Schwikowski, M., Abbaszade, G., Schnelle-Kreis, J., Zimmermann, R., An, Z., Szidat, S., Baltensperger, U., Haddad, I. E., and Prevot, A. S. H.: High secondary aerosol contribution to particulate pollution during haze events in China, Nature, 514, 218–222, doi:10.1038/nature13774, 2014.

Huang, X.-F., Yu, J. Z., He, L. Y., and Hu, M.: Size distribution characteristics of elemental carbon emitted from Chinese vehicles: results of a tunnel study and atmospheric implications, Environ. Sci. Technol., 40, 5355–5360, doi:10.1021/es0607281, 2006.

Huang, X.-F., He, L.-Y., Hu, M., Canagaratna, M. R., Sun, Y., Zhang, Q., Zhu, T., Xue, L., Zeng, L.-W., Liu, X.-G., Zhang, Y.-H., Jayne, J. T., Ng, N. L., and Worsnop, D. R.: Highly time-resolved chemical characterization of atmospheric submicron particles during 2008 Beijing Olympic Games using an Aerodyne High-Resolution Aerosol Mass Spectrometer, Atmos. Chem. Phys., 10, 8933–8945, doi:10.5194/acp-10-8933-2010, 2010.

Irwin, M., Good, N., Crosier, J., Choularton, T. W., and McFiggans, G.: Reconciliation of measurements of hygroscopic growth and critical supersaturation of aerosol particles in central Germany, Atmos. Chem. Phys., 10, 11737–11752, doi:10.5194/acp-10-11737-2010, 2010.

Jimenez, J. L., Canagaratna, M. R., Donahue, N. M., Prevot, A. S. H., Zhang, Q., Kroll, J. H., DeCarlo, P. F., Allan, J. D., Coe, H., Ng, N. L., Aiken, A. C., Docherty, K. S., Ulbrich, I. M., Grieshop, A. P., Robinson, A. L., Duplissy, J., Smith, J. D., Wilson, K. R., Lanz, V. A., Hueglin, C., Sun, Y. L., Tian, J., Laaksonen, A., Raatikainen, T., Rautiainen, J., Vaattovaara, P., Ehn, M., Kulmala, M., Tomlinson, J. M., Collins, D. R., Cubison, M. J., E, Dunlea, J., Huffman, J. A., Onasch, T. B., Alfarra, M. R., Williams, P. I., Bower, K., Kondo, Y., Schneider, J., Drewnick, F., Borrmann, S., Weimer, S., Demerjian, K., Salcedo, D., Cottrell, L., Griffin, R., Takami, A., Miyoshi, T., Hatakeyama, S., Shimono, A., Sun, J. Y., Zhang, Y. M., Dzepina, K., Kimmel, J. R., Sueper, D., Jayne, J. T., Herndon, S. C., Trimborn, A. M., Williams, L. R., Wood, E. C., Middlebrook, A. M., Kolb, C. E., Baltensperger, U., and Worsnop, D. R.: Evolution of organic aerosols in the atmosphere, Science, 326, 1525–1529, doi:10.1126/science.1180353, 2009.

Kanakidou, M., Seinfeld, J. H., Pandis, S. N., Barnes, I., Dentener, F. J., Facchini, M. C., Van Dingenen, R., Ervens, B., Nenes, A., Nielsen, C. J., Swietlicki, E., Putaud, J. P., Balkanski, Y., Fuzzi, S., Horth, J., Moortgat, G. K., Winterhalter, R., Myhre, C. E. L., Tsigaridis, K., Vignati, E., Stephanou, E. G., and Wilson, J.: Organic aerosol and global climate modelling: a review, Atmos. Chem. Phys., 5, 1053–1123, doi:10.5194/acp-5-1053-2005, 2005.

Kiselev, A., Wennrich, C., Stratmann, F., Wex, H., Henning, S., Mentel, T. F., Kiendler-Scharr, A., Schneider, J., Walter, S., and Lieberwirth, I.: Morphological characterization of soot aerosol particles during LACIS Experiment in November (LExNo), J. Geophys. Res.-Atmos., 115, D11204, doi:10.1029/2009jd012635, 2010.

Kondo, Y., Sahu, L., Moteki, N., Khan, F., Takegawa, N., Liu, X., Koike, M., and Miyakawa, T.: Consistency and traceability of black carbon measurements made by laser-induced incandescence, thermal-optical transmittance, and filter-based photo-absorption techniques, Aerosol Sci. Tech., 45, 295–312, doi:10.1080/02786826.2010.533215, 2011.

Kreidenweis, S. M. and Asa-Awuku, A.: 5.13 – Aerosol hygroscopicity: particle water content and its role in atmospheric processes, in: Treatise on Geochemistry, 2nd edn., edited by: Turekian, H. D. H. K., Elsevier, Oxford, 331–361, 2014.

Liu, P. F., Zhao, C. S., Göbel, T., Hallbauer, E., Nowak, A., Ran, L., Xu, W. Y., Deng, Z. Z., Ma, N., Mildenberger, K., Henning, S., Stratmann, F., and Wiedensohler, A.: Hygroscopic properties of aerosol particles at high relative humidity and their diurnal variations in the North China Plain, Atmos. Chem. Phys., 11, 3479–3494, doi:10.5194/acp-11-3479-2011, 2011.

Lopez-Yglesias, X. F., Yeung, M. C., Dey, S. E., Brechtel, F. J., and Chan, C. K.: Performance evaluation of the Brechtel Mfg. Humidified Tandem Differential Mobility Analyzer (BMI HTDMA) for studying hygroscopic properties of aerosol particles, Aerosol Sci. Tech., 48, 969–980, doi:10.1080/02786826.2014.952366, 2014.

Malm, W. C. and Kreidenweis, S. M.: The effects of models of aerosol hygroscopicity on the apportionment of extinction, Atmos. Environ., 31, 1965–1976, doi:10.1016/s1352-2310(96)00355-x, 1997.

Maßling, A., Wiedensohler, A., Busch, B., Neusüß, C., Quinn, P., Bates, T., and Covert, D.: Hygroscopic properties of different aerosol types over the Atlantic and Indian Oceans, Atmos. Chem. Phys., 3, 1377–1397, doi:10.5194/acp-3-1377-2003, 2003.

Massling, A., Stock, M., Wehner, B., Wu, Z. J., Hu, M., Brüggemann, E., Gnauk, T., Herrmann, H., and Wiedensohler, A.: Size segregated water uptake of the urban submicrometer aerosol in Beijing, Atmos. Environ., 43, 1578–1589, doi:10.1016/j.atmosenv.2008.06.003, 2009.

Massling, A., Niedermeier, N., Hennig, T., Fors, E. O., Swietlicki, E., Ehn, M., Hämeri, K., Villani, P., Laj, P., Good, N., McFiggans, G., and Wiedensohler, A.: Results and recommendations from an intercomparison of six Hygroscopicity-TDMA systems, Atmos. Meas. Tech., 4, 485–497, doi:10.5194/amt-4-485-2011, 2011.

McFiggans, G., Artaxo, P., Baltensperger, U., Coe, H., Facchini, M. C., Feingold, G., Fuzzi, S., Gysel, M., Laaksonen, A., Lohmann, U., Mentel, T. F., Murphy, D. M., O'Dowd, C. D., Snider, J. R., and Weingartner, E.: The effect of physical and chemical aerosol properties on warm cloud droplet activation, Atmos. Chem. Phys., 6, 2593–2649, doi:10.5194/acp-6-2593-2006, 2006.

McMurry, P. H., Wang, X., Park, K., and Ehara, K.: The relationship between mass and mobility for atmospheric particles: a new technique for measuring particle density, Aerosol Sci. Tech., 36, 227–238, doi:10.1080/027868202753504083, 2002.

Medina, J., Nenes, A., Sotiropoulou, R.-E. P., Cottrell, L. D., Ziemba, L. D., Beckman, P. J., and Griffin, R. J.: Cloud condensation nuclei closure during the International Consortium for Atmospheric Research on Transport and Transformation 2004 campaign: effects of size-resolved composition, J. Geophys. Res., 112, D10S31, doi:10.1029/2006jd007588, 2007.

Mei, F., Hayes, P. L., Ortega, A., Taylor, J. W., Allan, J. D., Gilman, J., Kuster, W., de Gouw, J., Jimenez, J. L., and Wang, J.: Droplet activation properties of organic aerosols observed at an urban site during CalNex-LA, J. Geophys. Res.-Atmos., 118, 2903–2917, doi:10.1002/jgrd.50285, 2013.

Park, K., Kittelson, D. B., Zachariah, M. R., and McMurry, P. H.: Measurement of inherent material density of nanoparticle agglomerates, J. Nanopart. Res., 6, 267–272, 2004.

Patrick Arnott, W., Moosmüller, H., Fred Rogers, C., Jin, T., and Bruch, R.: Photoacoustic spectrometer for measuring light absorption by aerosol: instrument description, Atmos. Environ., 33, 2845–2852, doi:10.1016/S1352-2310(98)00361-6, 1999.

Petters, M. D. and Kreidenweis, S. M.: A single parameter representation of hygroscopic growth and cloud condensation nucleus activity, Atmos. Chem. Phys., 7, 1961–1971, doi:10.5194/acp-7-1961-2007, 2007.

Pöschl, U.: Atmospheric aerosols: composition, transformation, climate and health effects, Angew. Chem. Int. Edit., 44, 7520–7541, 2005.

Potukuchi, S. and Wexler, A. S.: Identifying solid-aqueous phase transitions in atmospheric aerosols – I. Neutral-acidity solutions, Atmos. Environ., 29, 1663–1676, doi:10.1016/1352-2310(95)00074-9, 1995.

Sloane, C. S. and Wolff, G. T.: Prediction of ambient light scattering using a physical model responsive to relative humidity: validation with measurements from detroit, Atmos. Environ., 19, 669–680, doi:10.1016/0004-6981(85)90046-0, 1985.

Stokes, R. H. and Robinson, R. A.: Interactions in aqueous nonelectrolyte solutions. I. Solute-solvent equilibria, J. Phys. Chem.-US, 70, 2126–2130, 1966.

Swietlicki, E., Zhou, J., Berg, O. H., Martinsson, B. G., Frank, G., Cederfelt, S.-I., Dusek, U., Berner, A., Birmili, W., Wiedensohler, A., Yuskiewicz, B., and Bower, K. N.: A closure study of sub-micrometer aerosol particle hygroscopic behaviour, Atmos. Res., 50, 205–240, doi:10.1016/s0169-8095(98)00105-7, 1999.

Swietlicki, E., Hansson, H. C., Hämeri, K., Svenningsson, B., Massling, A., McFiggans, G., McMurry, P. H., Petäjä, T., Tunved, P., Gysel, M., Topping, D., Weingartner, E., Baltensperger, U., Rissler, J., Wiedensohler, A., and Kulmala, M.: Hygroscopic properties of submicrometer atmospheric aerosol particles measured with H-TDMA instruments in various environments – a review, Tellus B, 60, 432–469, doi:10.1111/j.1600-0889.2008.00350.x, 2008.

Tang, I. N. and Munkelwitz, H. R.: Water activities, densities, and refractive indices of aqueous sulfates and sodium nitrate droplets of atmospheric importance, J. Geophys. Res., 99, 18801–18808, doi:10.1029/94jd01345, 1994.

Ulbrich, I. M., Canagaratna, M. R., Zhang, Q., Worsnop, D. R., and Jimenez, J. L.: Interpretation of organic components from Positive Matrix Factorization of aerosol mass spectrometric data, Atmos. Chem. Phys., 9, 2891–2918, doi:10.5194/acp-9-2891-2009, 2009.

Varutbangkul, V., Brechtel, F. J., Bahreini, R., Ng, N. L., Keywood, M. D., Kroll, J. H., Flagan, R. C., Seinfeld, J. H., Lee, A., and Goldstein, A. H.: Hygroscopicity of secondary organic aerosols formed by oxidation of cycloalkenes, monoterpenes, sesquiterpenes, and related compounds, Atmos. Chem. Phys., 6, 2367–2388, doi:10.5194/acp-6-2367-2006, 2006.

Virkkula, A., Van Dingenen, R., Raes, F., and Hjorth, J.: Hygroscopic properties of aerosol formed by oxidation of limonene, α-pinene, and β-pinene, J. Geophys. Res., 104, 3569–3579, doi:10.1029/1998jd100017, 1999.

Wu, Z. J., Nowak, A., Poulain, L., Herrmann, H., and Wiedensohler, A.: Hygroscopic behavior of atmospherically relevant water-soluble carboxylic salts and their influence on the water uptake of ammonium sulfate, Atmos. Chem. Phys., 11, 12617–12626, doi:10.5194/acp-11-12617-2011, 2011.

Wu, Z. J., Poulain, L., Henning, S., Dieckmann, K., Birmili, W., Merkel, M., van Pinxteren, D., Spindler, G., Müller, K., Stratmann, F., Herrmann, H., and Wiedensohler, A.: Relating particle hygroscopicity and CCN activity to chemical composition during the HCCT-2010 field campaign, Atmos. Chem. Phys., 13, 7983–7996, doi:10.5194/acp-13-7983-2013, 2013.

Ye, X., Tang, C., Yin, Z., Chen, J., Ma, Z., Kong, L., Yang, X., Gao, W., and Geng, F.: Hygroscopic growth of urban aerosol particles during the 2009 Mirage-Shanghai Campaign, Atmos. Environ., 64, 263–269, doi:10.1016/j.atmosenv.2012.09.064, 2013.

Zdanovskii, B.: Novyi Metod Rascheta Rastvorimostei Elektrolitov v Mnogokomponentnykh Sistema, Zh. Fiz. Khim.+, 22, 1478–1485, 1486–1495, 1948.

Zhang, J., Wang, L., Chen, J., Feng, S., Shen, J., and Jiao, L.: Hygroscopicity of ambient submicron particles in urban Hangzhou, China, Front. Environ. Sci. Eng. China, 5, 342–347, doi:10.1007/s11783-011-0358-7, 2011.

Table 1. Gravimetric densities (ρ) and hygroscopicity parameters (κ) used in this study.

Species	NH_4NO_3	NH_4HSO_4	$(NH_4)_2SO_4$	SOA	POA	BC
[$kg\,m^{-3}$]	1720	1780	1769	1400	1400	1700
κ	0.58	0.56	0.48	0.1	0	0

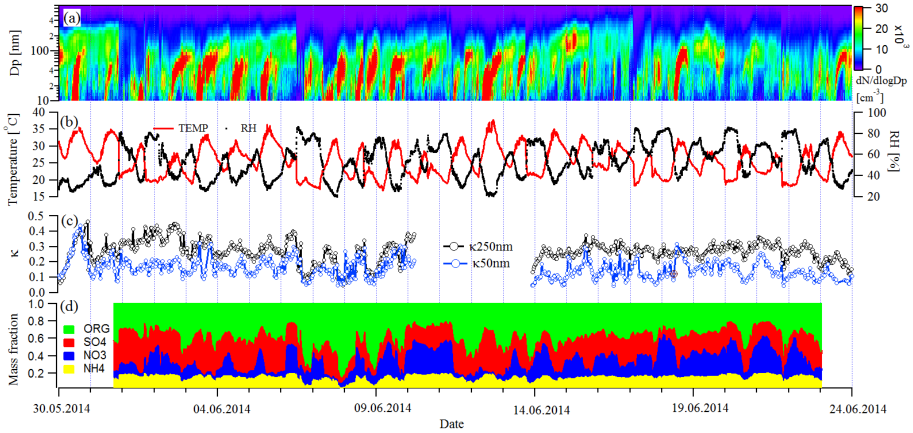

Figure 1. Time series of particle number size distribution, ambient temperature and relative humidity, hygroscopicity parameters, and chemical composition of NR-PM_1 during the measuring period.

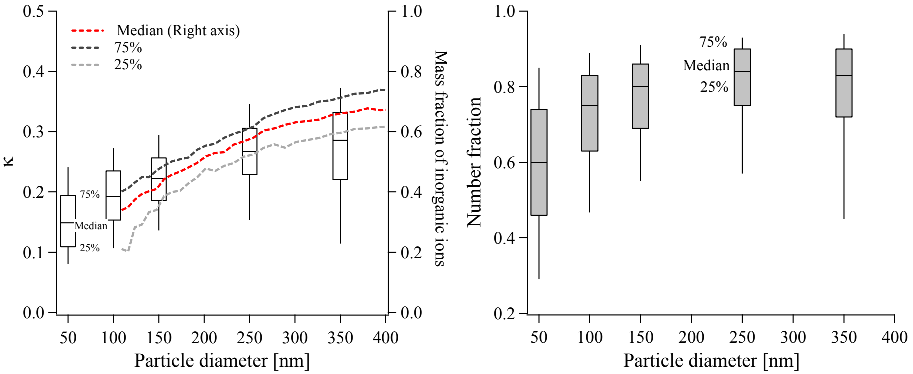

Figure 2. Size-resolved particle hygroscopicity and mass fraction of organics (left) and Size-dependent number fraction of hydrophilic mode (right).

Title Page
Abstract
Introduction
Conclusions
References
Tables
Figures
◀◀
▶▶
◀
▶
Back
Close
Full Screen / Esc
Printer-friendly Version
Interactive Discussion

ACPD
15, 11495–11524, 2015

Particle hygroscopicity in the atmosphere of Beijing, China

Z. J. Wu et al.

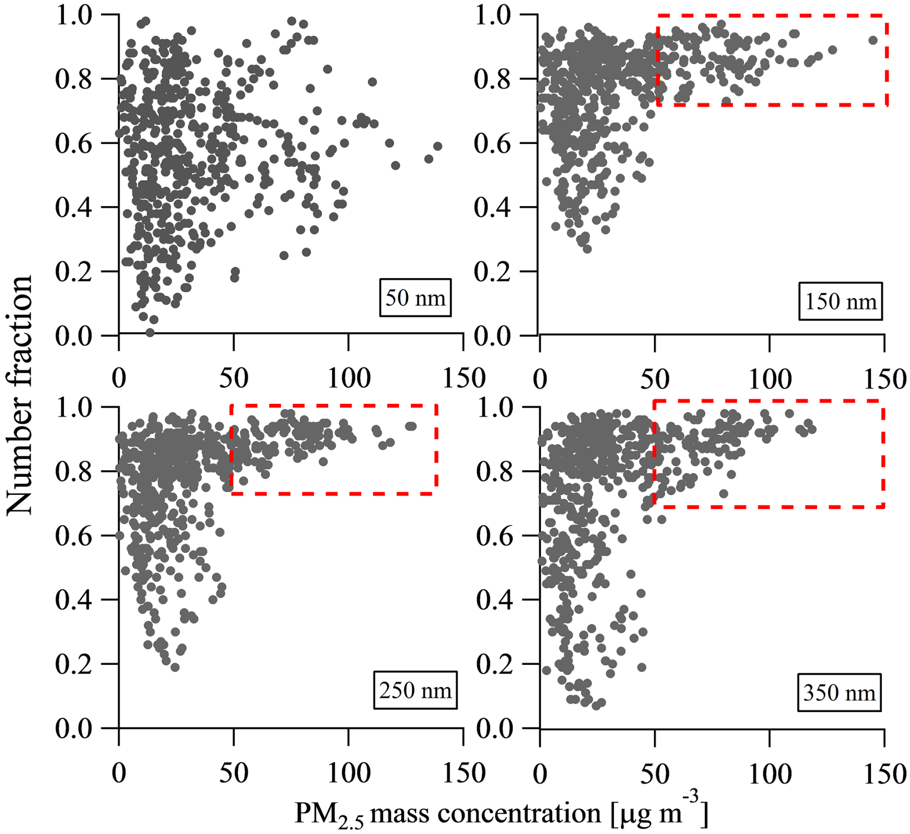

Figure 3. Number fraction of hydrophilic mode vs. $PM_{2.5}$ mass concentration.

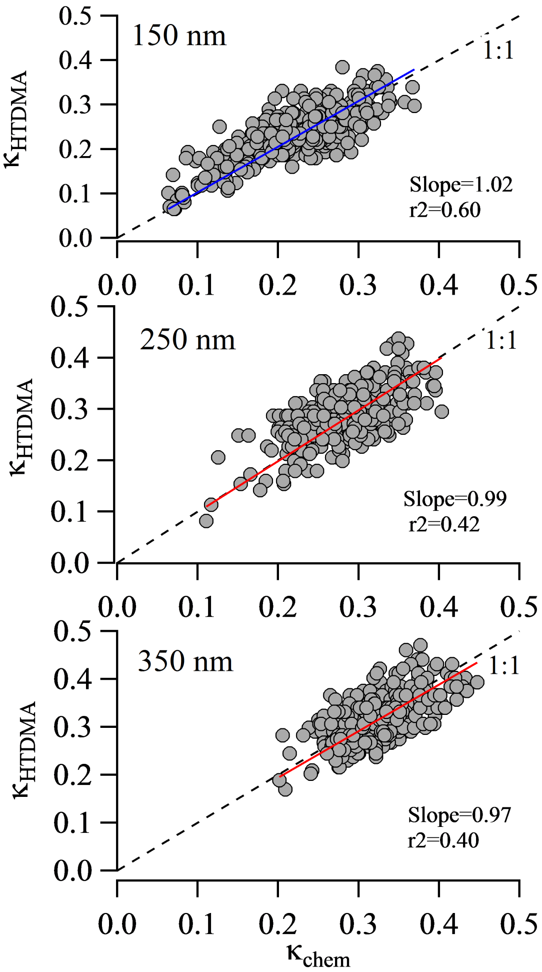

Figure 4. κ_{HTDMA} vs. κ_{chem} using size-resolved chemical composition data.

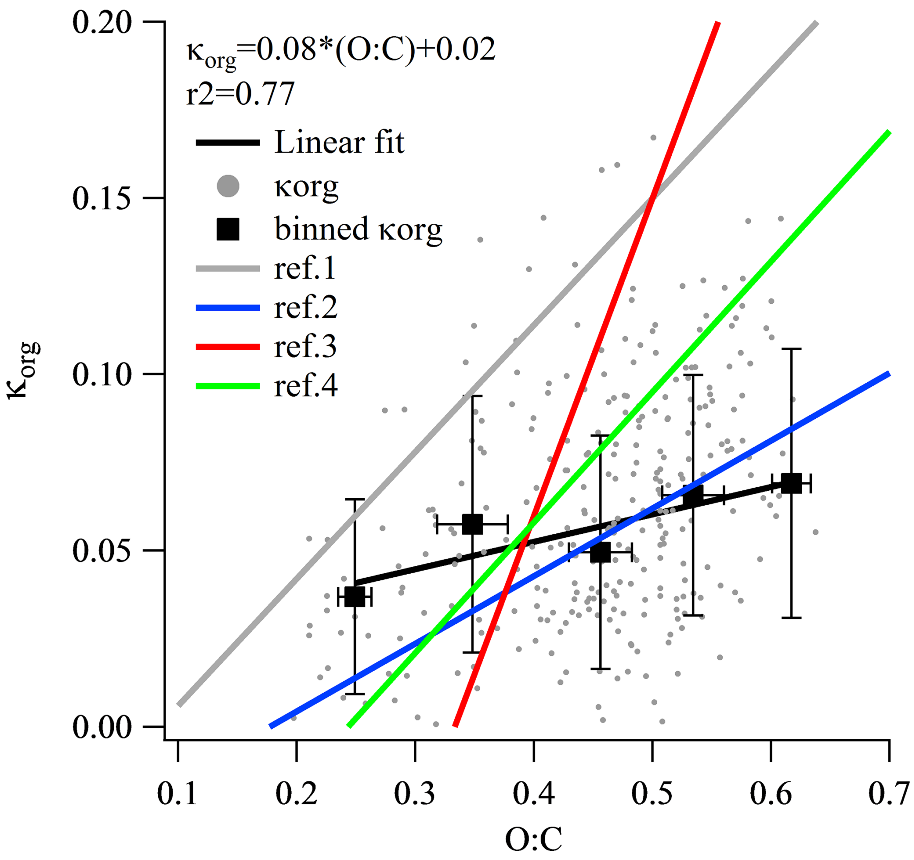

Figure 5. The relationship between organic hygroscopicity parameter (κ_{org}) and oxygen to carbon ratio (O : C). ref.1: Kanpur, India (Bhattu and Tripathi, 2015), ref.2: a forest site, Germany (Wu et al., 2013), ref.3: a rural site in Ontario, Canada, (Chang et al., 2010), ref.4: an urban site in Pasadena, California (Mei et al., 2013).

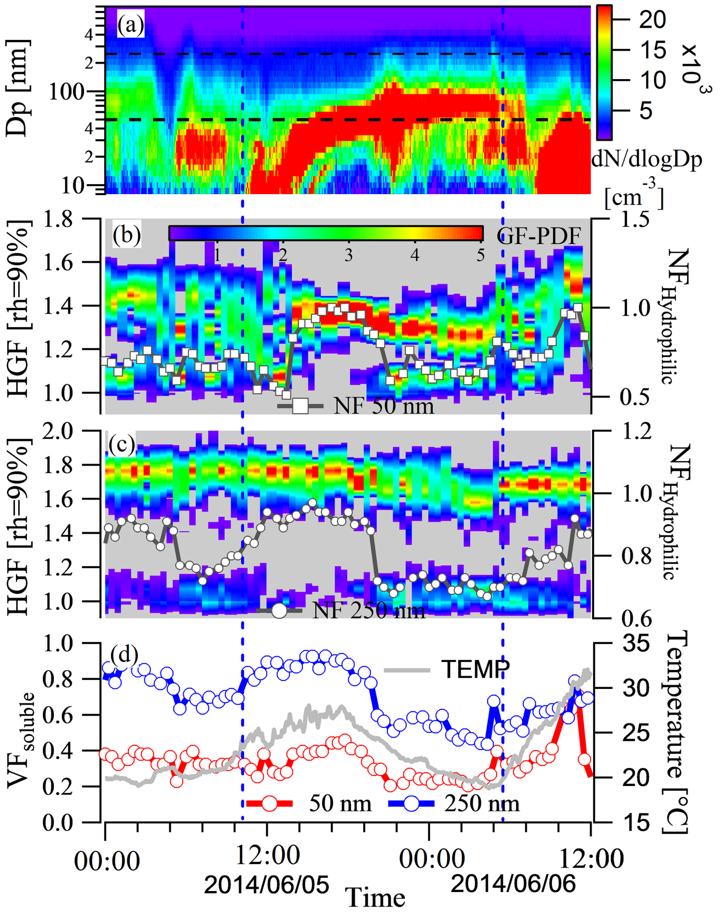

Figure 6. The variation in particle hygroscopicity during new particle formation event. HGF: hygroscopic growth factor, $NF_{Hydrophilic}$: number fraction of hydrophilic mode particle, $VF_{soluble}$: water soluble volume fraction.